JACS
JOURNAL OF THE AMERICAN CHEMICAL SOCIETY
Article
pubs.acs.org/JACS

Design and Synthesis of Epicocconone Analogues with Improved Fluorescence Properties

Philippe A. Peixoto,[†] Agathe Boulangé,[†] Malcolm Ball,[‡] Bertrand Naudin,[§] Thibault Alle,[†] Pascal Cosette,[§] Peter Karuso,*[,‡] and Xavier Franck*[,†]

[†]Normandie Université, COBRA, UMR 6014 & FR 3038; Université de Rouen; INSA Rouen; CNRS, 1 rue Tesnière, 76821 Mont-Saint-Aignan Cedex, France

[‡]Department of Chemistry and Biomolecular Sciences, Macquarie University, Sydney, NSW 2109, Australia

[§]CNRS UMR 6270, PBS & FR3038, Plateforme Protéomique PISSARO, Université de Rouen, 76821 Mont-Saint-Aignan, France

Supporting Information

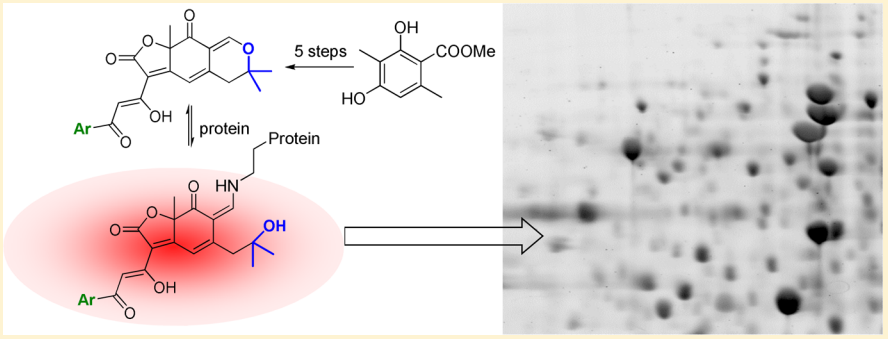

ABSTRACT: Epicocconone is a natural latent fluorophore that is widely used in biotechnology because of its large Stokes shift and lack of fluorescence in its unconjugated state. However, the low photostability and quantum yields of epicocconone have limited its wider use, and in the absence of a total synthesis, this limitation has been a long-standing problem. Here we report a general strategy for the synthesis of epicocconone analogues that relies on a 2-iodoxybenzoic acid-mediated dearomatization and on the replacement of the triene tail of the natural product by an aromatic ring. This design element is general and the synthesis is straightforward, providing ready access to libraries of polyfunctional fluorophores with long Stokes shifts based on the epicocconone core. Our structural modifications resulted in analogues with increased photostability and quantum yields compared with the natural product. Staining proteomic gels with these new analogues showed significant lowering of the detection limit and a 30% increase in the number of low-abundance proteins detected. These epiccoconone analogues will substantially improve the discovery rate of biomarker needles in the proteomic haystack.

INTRODUCTION

The power of fluorescent probes can be enhanced by controlling how and when the probe becomes excitable. Such latent fluorophores result in high specificity and low background and thus high sensitivity. Most latent fluorophores either react covalently with their target[1] or work by the removal of a protecting group[2] or quenching group[3] and are thus irreversible. However, random covalent modification of target biomolecules is generally incompatible with proteomics (where protein identification relies on mass spectrometry of peptides released by tryptic digestion) unless considerable effort is expended in modifying the bioinformatics software.[4] This is especially true of small molecules that modify lysine residues, as these are no longer recognized by trypsin. Trypsin digestion of single proteins or proteomes is the stalwart of protein identification by mass spectrometry. Covalent modification of biomolecules is also of limited use in live-cell applications, where covalent modification by xenobiotics is often toxic.

The recent discovery of the natural product epicocconone (**1**) from the fungus *Epicoccum nigrum*[5] revealed the first reversible-covalent latent fluorophore, which has found wide biotechnological applications in Western blotting, proteomic gel staining, protein quantification, live-cell imaging, and monitoring of enzymatic activity.[6] Mechanism of action studies revealed that the masked aldehyde of epicocconone reacts with amine residues (e.g., lysine residues in proteins) to create a red-fluorescent enamine that forms an internal charge transfer complex that is stable at pH 2.4 (Scheme 1) and highly emissive in the red (610 nm).[7]

Epicocconone is unique in that at neutral pH the fluorophore reverts back to the nonfluorescent masked aldehyde in a base-catalyzed reaction (Scheme 1), providing traceless detection of proteins in a variety of formats.[7,8] The compound is also freely

Received: July 9, 2014
Published: October 1, 2014

   dx.doi.org/10.1021/ja506914p | J. Am. Chem. Soc. 2014, 136, 15248−15256

Scheme 1. Mechanism of the Reversible Reaction of Epicocconone (1) with Proteins To Produce a Highly Fluorescent Enamine

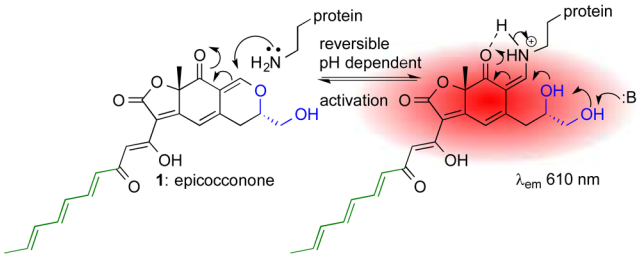

water-soluble yet cell-permeable and has a large Stokes shift. Few small molecules have been found that emit in the red upon irradiation in the UV or blue, even though such a property has been identified as having great importance in dual staining methods.[9] Compounds that fall into this class include dapoxyl-(2-aminoethyl)sulfonamide, Fura Red, Sypro Ruby, and di-8-ANEPPS (Scheme 2), but none of these combine a large Stokes

Scheme 2. Examples of Dyes Excited in the Near-UV/Blue and Emitting in the Orange/Red Region

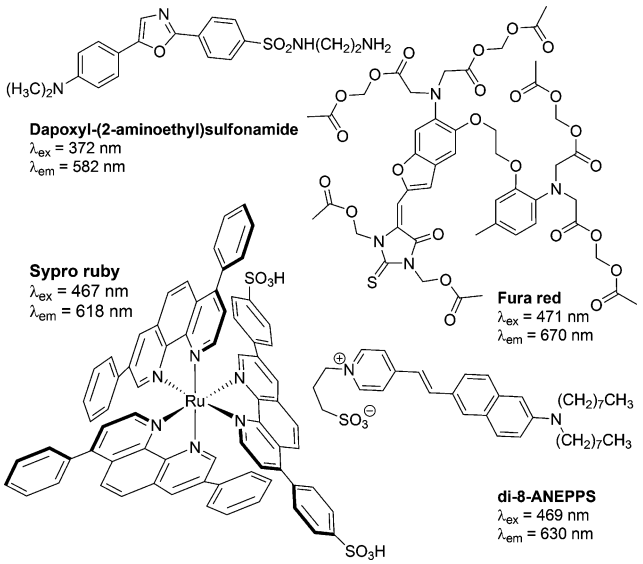

shift with the "turn on"/"turn off" capacity of epicocconone.[10] A large Stokes shift is advantageous because it minimizes interference from intrinsic fluorescence and Rayleigh scattering as well as self-quenching when two or more fluorophores are within the Förster radius. However, epicocconone suffers from photobleaching when used, for example, over a transilluminator for manual spot picking in 2D gel electrophoresis.[11] This may be due to photooxidation/photoisomerization[12] of the triene tail or photooxidation of the alcohols.[13]

As proteomes are highly complex with a large dynamic range of protein concentration, it is imperative that new tools be developed for identifying and quantifying low-abundance proteins because of their pharmaceutical, diagnostic, and medical value.[14] Methods that allow deeper interrogation of a proteome than current methods are thus in high demand, as all of the new proteins seen are, by definition, low-abundance proteins. This challenge inspired us to investigate the design and synthesis of new fluorophores that encompass the advantages of **1** but have improved photophysical properties such as increased quantum yield and photostability.

RESULTS AND DISCUSSION

The design of more potent analogues of **1** hinged on replacing the triene tail with an isosteric aromatic ring and the ring-C alcohol with a dimethyl group (Scheme 3; shown in green and

Scheme 3. Retrosynthetic Analysis

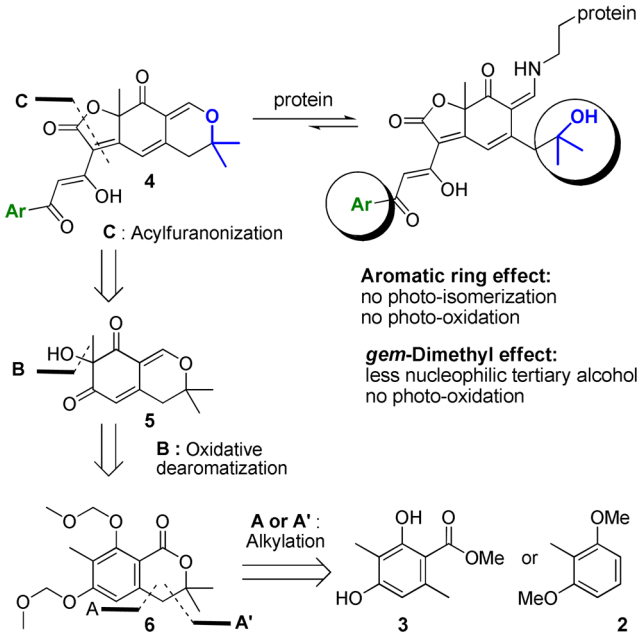

blue, respectively). These modifications should have no effect on the fluorescent scaffold but avoid photoisomerization or photooxidations that could lead to decomposition, thereby reducing the photobleaching observed for the natural product. It has also been suggested that photoisomerization of the triene tail is the major nonradiative decay mechanism for **1** in solution, leading to a low quantum yield.[8a] Furthermore, the geminal disubstitution on the C ring should reduce the rate of recyclization to the masked aldehyde by replacing the 1,2-diol (shown in blue in Scheme 1) with a less nucleophilic (more hindered) tertiary alcohol.

Retrosynthetically, analogues of epicocconone could be won from simple starting materials such as 2-methylresorcinol dimethyl ether (**2**) or methyl atratate (**3**) through three key steps (Scheme 3). The tricyclic core of epicocconone **4** could be synthesized by trapping of an acyl ketene by **5** with concomitant intramolecular Knoevenagel condensation in a one-pot procedure (step C). In turn, **5** could be envisaged as an oxidation product of **6** (step B), which in turn could be readily prepared from either commercially available **2** or **3** by alkylation (step A or A′).

Two strategies for the synthesis of lactone **6** were successful (Scheme 4). Our first strategy started with the formation of amide **7** by the reaction of **2** with *i*PrNCO in the presence of $AlCl_3$. Directed *ortho* metalation of amide **7** using 2 equiv of *tert*-butyllithium complexed in situ with tetramethylethylenediamine (TMEDA) and subsequent reaction of the transient aryllithium species with 2,2-dimethyloxirane produced **8** and introduced the *gem*-dimethyl group. Lactonization of amido alcohol **8** was achieved by refluxing in toluene with

dx.doi.org/10.1021/ja506914p | J. Am. Chem. Soc. 2014, 136, 15248−15256

Scheme 4. Synthesis of 6 via Two Different Routes[a]

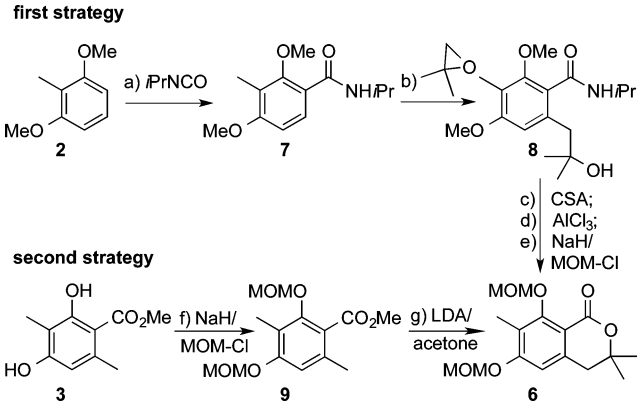

[a]Reagents and conditions: (a) *i*PrNCO (1.25 equiv), $AlCl_3$ (1.05 equiv), CH_2Cl_2, 0 °C, 3 h, 95%. (b) TMEDA (2.0 equiv), *t*-BuLi (2.2 equiv), THF, −15 °C, 30 min, then 2,2-dimethyloxirane (2.2 equiv), 25 °C, 1.5 h, 92%. (c) CSA (1.2 equiv), toluene, reflux, 2 h, 76%. (d) $AlCl_3$ (10.0 equiv), CH_2Cl_2, reflux, 20 h, 99%. (e) NaH (2.0 equiv), MOM-Cl (5.0 equiv), THF, 25 °C, 2 h, 100%. (f) NaH (3.0 equiv), MOM-Cl (3.0 equiv), THF, 25 °C, 3 h, 87%. (g) DIPA (1.0 equiv), *n*-BuLi (1.0 equiv), THF, −78 °C, 30 min, then acetone (0.8 equiv), 5 min, 60%.

camphorsulfonic acid (CSA). Finally the phenol protecting group was swapped from methyl to methoxymethylene (MOM) to yield **6** in two steps. The second, shorter strategy started with MOM protection of **3** before regioselective formation of the benzylic anion of **9** by treatment with lithium diisopropylamide (LDA) at low temperature. The *gem*-dimethyl group was then introduced by the addition of freshly distilled acetone to the anion. While the first longer route (five steps) gave a high overall yield of 66%, the shorter second route was only two steps but offered a slightly lower overall yield of 52%. Both routes are quite practical and suitable for multigram-scale synthesis of **6**.

The next key intermediate **5** (Scheme 5) was obtained by first reducing **6** to hemiacetal **10** with diisobutylaluminum hydride (DIBAL). The reaction proceeded quantitatively in toluene, but all other solvents led to over-reduction and isolation of mixtures containing the diol. Treatment of hemiacetal **10** with the λ5-iodinane derivative 2-iodoxybenzoic acid (IBX) in the presence of trifluoroacetic acid (TFA) and water deprotected the MOM ethers, dehydrated the hemiacetal to the oxonium ion (as observed by NMR), and effected *ortho* dearomatization.[15] The addition of water was essential in this reaction as it increased the yield and rate of reaction and prevented the formation of TFA esters.[16] Under these conditions, the second key intermediate **5** was obtained in an overall yield of 68% from **6**.

Analogues of **1** bearing a ketone side chain could be synthesized from **5** by reaction with an acyl ketene.[17] The intermediate β-keto esters could then undergo Knoevenagel condensations through **11** or **11′** to yield either 6,7-furanone **12** or 7,8-furanone **13**, respectively (Scheme 6).

Scheme 5. Synthesis of 5 by Oxidative Dearomatization[a]

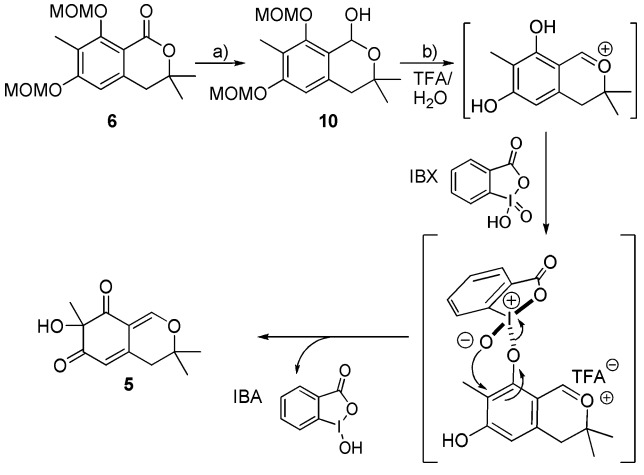

[a]Reagents and conditions: (a) DIBAL (1.3 equiv), toluene, −78 °C, 20 min. (b) TFA (7.0 equiv), water (20 equiv), IBX (2.0 equiv), CH_2Cl_2, 25 °C, 3 h, 68% over two steps.

Scheme 6. Reaction of 5 with in Situ-Generated Acyl Ketenes Followed by Knoevenagel Cyclization

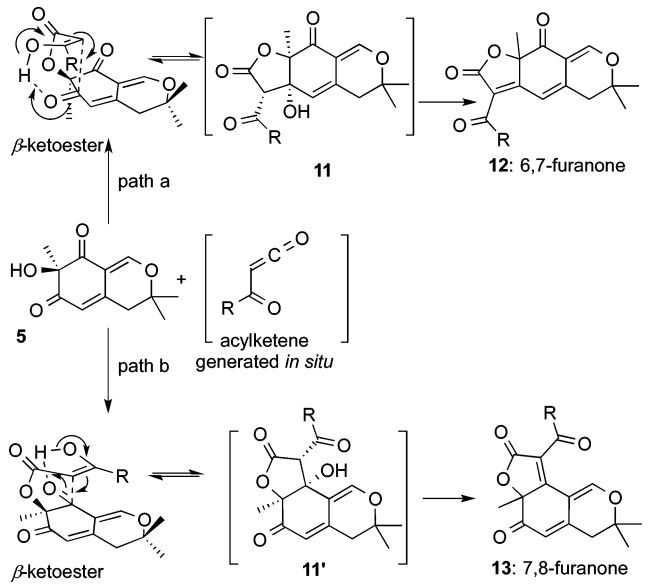

The one-pot installation of the acyl furanone could be envisaged through trapping of an acyl ketene formed from thermal fragmentation of dioxin-4-ones **14** by the alcohol of **5**.[16a,18] A library of analogues could be synthesized through this route simply by starting with different carboxylic acids (Scheme 7). In practice, the synthesis of **14** proceeded smoothly via condensation of the lithium enolate of *tert*-butyl acetate with Weinreb amides. The reaction of the resulting β-keto esters with acetone in acidic conditions yielded the dioxinones in 71−82% yield (Scheme 7). The reaction of **14a** with **5** at 110 °C in the presence of triethylamine gave 6,7-furanone **12a** in 86% yield with no isolatable amount of the undesired 7,8-regioisomer **13a** arising from path b in Scheme 6. Starting with different dioxinones, compounds **12a−d** were obtained. However, when R was an alkyl chain (e.g., **14c**), mixtures were obtained with the undesired regioisomer **13c** being the major product. This unexpected reversal of regioselectivity warranted further investigation.

After the reaction of the acyl ketenes with **5**, for cyclization to the acyl furanone to occur, the enolized side chain must adopt a suitable conformation that allows cyclization with concomitant proton transfer (Scheme 6). Two possible transition states

dx.doi.org/10.1021/ja506914p | J. Am. Chem. Soc. 2014, 136, 15248−15256

Scheme 7. Synthesis of Epicocconone Analogues from 5 and Dioxinones 14[a]

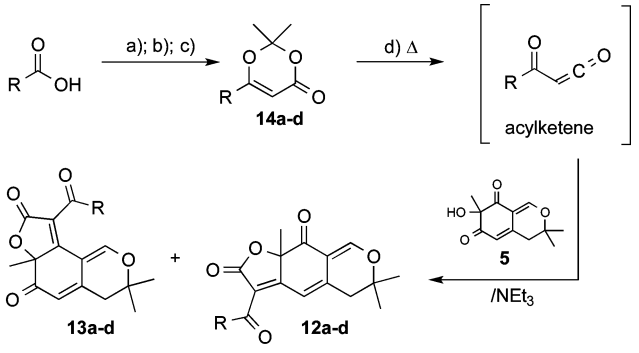

	R	12	13
a	*p*-anisyl	86%	<2%
b	2-naphthyl	64%	<2%
c	*n*-heptyl	20%	30%
d	phenyl	60%	<2%

[a]Reagents and conditions: (a) $(COCl)_2$ (1.25 equiv), CH_2Cl_2/DMF (cat.), 1.5 h; solvent removal, HN(Me)OMe (1.4 equiv) then Et_3N (1.0 equiv), CH_2Cl_2, 2 h, 86–96% yield over two steps. (b) DIPA (2.0 equiv), BuLi (2.0 equiv)/THF, −78 °C, then *t*-BuOAc (3 equiv), 1 h, 91–99% yield. (c) Ac_2O (15 equiv), H_2SO_4 (1 equiv)/acetone, 0–25 °C over 45 min, 71–82% yield. (d) **5** (0.67 equiv), Et_3N (1.33 equiv), molecular sieves (4 Å; 200 mg/mmol)/toluene, 110 °C, 3 h.

could be envisaged, one leading to the 6,7-furanone (path a) and the other to the 7,8-furanone (path b). The steric requirements, if R is aryl, are greater for path b, as in the transition state (TS) the R group lies over the pyran ring and interacts directly with the *gem*-dimethyl group. However, if R is alkyl, this steric hindrance is reduced because of the flexibility and smaller size of the side chain compared with an aryl group. In both cases, a concerted mechanism must produce the all-*cis* γ-lactone (**11** or **11′**), which is set up for a facile syn elimination of water to give the respective furanone (**12** or **13**). This was confirmed by molecular modeling (Figure S1 in the Supporting Information). This qualitative model predicts a preference for **12** over **13** if R is aryl and less of a preference if R is alkyl. This was what was observed, except that with alkyl groups the undesired 7,8-furanone **13** was the major product, suggesting that other forces were at play.

To investigate this further, we performed density functional theory (DFT) calculations (DFT-D3//BP-86/TZVPP)[19] using a continuum solvent model (COSMO)[20] for toluene on the intermediate all-*cis* γ-lactones (**11** and **11′**; R = Et and Ph). Under the cyclization conditions (toluene, 110 °C), one would expect the thermodynamic products to dominate if the intramolecular Knoevenagel condensation is reversible (Scheme 6). Frequency calculations on the geometry-optimized intermediates (**11** and **11′**) confirmed that all of the predicted conformations were stationary points, and thermochemical properties were calculated at 383 K using Turbomole (Table 1). Gibbs free energy calculations predicted that the **12d**:**13d** ratio would be 1:0.5 while the **12c**:**13c** ratio would be 0.8:1. The latter is close to the experimental result (Scheme 7), while the former predicts the correct major product but the reaction is actually more selective for the desired regioisomer, suggesting that TS influences (Scheme 6 and Figure S1 in the Supporting Information) may also play a role in the observed product distribution. The differences in Gibbs free energy are predominately due to differences in entropy (Table 1). When

Table 1. Thermodynamic Properties of 11 and 11′ Based on High-Level DFT Calculations

	R	Gibbs free energy (kJ/mol)	entropic energy[a] (kJ/mol)	Boltzmann distribution[b]
11	Ph	739.91	306.89	0.66
11′	Ph	742.06	304.10	0.33
11	Et	689.37	285.71	0.45
11′	Et	688.69	286.35	0.55

[a]At 383 K using the Turbomole *freeh* package. [b]Based on differences in the Gibbs free energies of **11** and **11′**.

R is Ph, **11** has a higher entropic energy ($\Delta T\Delta S$ = 2.8 kJ/mol) while when R is Et, **11′** has the higher entropy ($\Delta T\Delta S$ = 0.6 kJ/mol) relative to **11** at 383 K.

In terms of spectral characteristics, compounds **12a–d** have low extinction coefficients (2000–4000 M^{-1} cm^{-1}) and low quantum yields (Table 2), and their excitation and emission curves are blue-shifted by ∼20 nm compared with those of epicocconone.[8a] Fluorescence data were obtained in 0.1% SDS at pH 2.5 to mimic the environment in an SDS-PAGE electrophoresis gel after fixing. While analogues **12a–d** did react with protein in water to yield a fluorescent enamine, the quantum yield increased only slightly. Analogue **12c**, with an aliphatic side chain, is ∼10 times less fluorescent than **12a**, and its regioisomer **13c** is completely devoid of any fluorescence.

While no useful probes arose from this work, it was now clear that the 6,7-furanone and the β-diketone were critical design features that needed to be incorporated to produce useful new fluorophores. In order to access analogues incorporating the β-diketone side chain, as in the natural product, we designed dioxin-4-ones **15**, which could be prepared by condensation of the lithium enolate of commercially available 2,2,6-trimethyl-4*H*-1,3-dioxin-4-one with various acyl chlorides (Scheme 8). Unfortunately, thermal fragmentation of **15d** under the same basic reaction conditions as with dioxin-4-ones **14** (vide supra) resulted in none of the desired product **4d**, presumably because of intramolecular trapping of the ketene to form 2-pyranones. The solution to this problem was simply to add Et_3N only after ketene formation and trapping with **5**. Even though the level of conversion for this reaction was quite high (∼70% by NMR) the isolated yield was moderated because of partial decomposition on silica gel. Again, only the desired 6,7-furanones **4a–d** bearing aryl moieties and enolized 1,3-diketones were obtained (Scheme 8). Methylated dioxinones **16** were prepared from **15** using methyl iodide followed by protection of the aryl ketone as the silyl ether. Reaction with **5** yielded **17** with a non-enolized 1,3-diketone in the same moderate yields (Scheme 8).

Although the isolated yields of **4** and **17** were moderate, this one-pot procedure performed four steps in one: fragmentation of β-keto dioxin-4-one **15** or **16** to a putative β-keto acyl ketene, acylation of **5**, cyclization, and finally dehydration exclusively to give the desired 6,7-furanone skeleton of epicocconone. The yields for this step could not be improved because β-keto acyl ketenes are unstable intermediates that are prone to cyclize to the 6-aryl-4-hydroxy-2*H*-pyran-2-ones or react with traces of water leading to β-keto acids, which easily decarboxylate.[14b] However, this method is step-economical, general, and achievable on a gram scale.

With several analogues in hand, we set out to characterize their fluorescence behavior (Figure 1 and Table 2). In the case of analogues **17a** and **17d**, the non-enolized 1,3-diketones were obtained and had emission wavelengths similar to those of

dx.doi.org/10.1021/ja506914p | J. Am. Chem. Soc. 2014, 136, 15248–15256

Scheme 8. Synthesis of Epicocconone Analogues from 5 and Dioxinones 15 and 16[a]

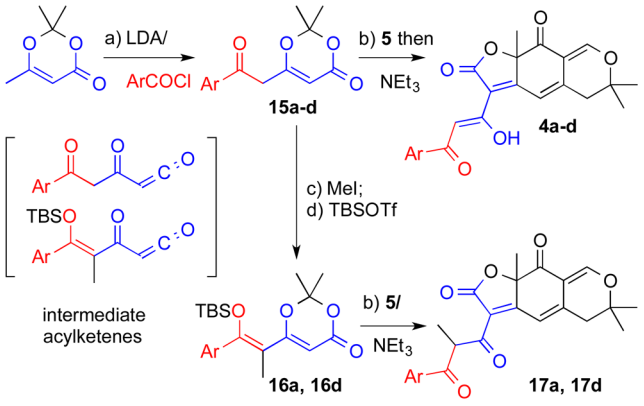

R	4	17
a: *p*-anisyl	30%	25%
b: 2-naphthyl	33%	
c: 6-chloro-3-pyridyl	27%	
d: phenyl	35%	29%

[a]Reagents and conditions: (a) DIPA (2.0 equiv), *n*-BuLi (2.0 equiv), THF, −78 °C, 30 min, then ArCOCl (1.0 equiv), −40 °C, 2 h, 41−62% yield. (b) **5** (0.67 equiv), molecular sieves (4 Å; 200 mg/mmol), toluene, 110 °C, 20 min, then Et_3N (1.33 equiv), 1 h, 27−35% yield. (c) K_2CO_3 (5.0 equiv), MeI (2.0 equiv), acetone, reflux, 2 h. (d) TBSOTf (1.5 equiv), DIEA (3.0 equiv), CH_2Cl_2, 25 °C, 2 h, 99% yield over two steps. (e) **5** (0.67 equiv), Et_3N (1.33 equiv), molecular sieves (4 Å; 200 mg/mmol), toluene, 110 °C, 3 h, 25−29%.

12a−d (i.e., blue-shifted by ∼20 nm compared with **1**) and low quantum yields. This indicated that the second carbonyl in **17** is not part of the chromophore. In contrast, analogues **4a−d** were obtained in the keto−enol form (from NMR) and exhibited excitation and emission spectra very similar to those of **1**, confirming that the triene tail is not required for strong fluorescence but that the *β*-keto−enol is.

In most cases, the formation of the enamines of **4** (with protein) resulted in dramatic increases in fluorescence and concomitant red shifts in the excitation and emission frequencies arising from increased conjugation, higher dipole moment in the excited state (Figure 1), and an increased charge transfer distance compared with the first series of analogues **12a−d**.[21] The exception to this was **4c**, which was more fluorescent in water ($\Phi_F \approx 40\%$) than in the presence of protein ($\Phi_F \approx 17\%$).

Interestingly, while all of the compounds except **13** were fluorescent and displayed one emission line, most displayed three distinct excitation maxima corresponding to S_0-S_3, S_0-S_2, and S_0-S_1 transitions (Table 2).

The advantage of **1** in protein detection is that it is virtually nonfluorescent in water ($\Phi_F < 1\%$), a characteristic shared with **4a** and **4d**.[22] However, in 0.1% SDS solution (Table 2), the quantum yields increase by an order of magnitude. This is presumably due to rigidification of the fluorophore in the viscous environment around SDS clusters and/or a reduction in collisional quenching from water. In contrast, **4b** and **4c** have considerably higher fluorescence than **1** in water[22] and in 0.1% SDS (Figure 1A).

The pyridyl analogue (**4c**) that seemed quite promising produced an enamine with bovine serum albumin (BSA) that was much less fluorescent than that of **1**. Compounds **4a** and **4d** were also less fluorescent than **1** in the presence of excess protein (Figure 1B), and this translated into inferior protein stains (Figure S7 in the Supporting Information). In the presence of excess protein, only **4b** matched **1** in fluorescence performance (Figure 1B), and it was selected for further study.

The application of **4a−d** for staining of proteins in electrophoresis gels was tested using 1D gels (Figure S7 in the Supporting Information) and 2D gels (Figure S9 in the Supporting Information), and the results confirmed that compound **4b** had the best protein staining characteristics. We chose to analyze the performance of **4b** in more detail by comparison with (1) Deep Purple Total Protein Stain[23] because Deep Purple contains **1** as its active ingredient and (2) Sypro Ruby[24] because it is the most popular fluorescent gel stain but is based on very different chemistry (Scheme 2). Analysis of serial dilutions of standard proteins (Figure 2) indicated that **4b** gave much darker staining and was generally twice as sensitive as the commercial products in 1D gels (Table 3 and Figure S6 in the Supporting Information), achieving picogram (low femtomolar) sensitivity. As both Deep Purple and **4b** are end-point stains, this difference is not related to staining times or protocols. We used the standard Deep Purple protocol in both cases and made no attempt to optimize the protocol for **4b**.

Similar results were obtained in the more critical 2D gel electrophoresis (Figure 3), where **4b** was able to reveal 33%

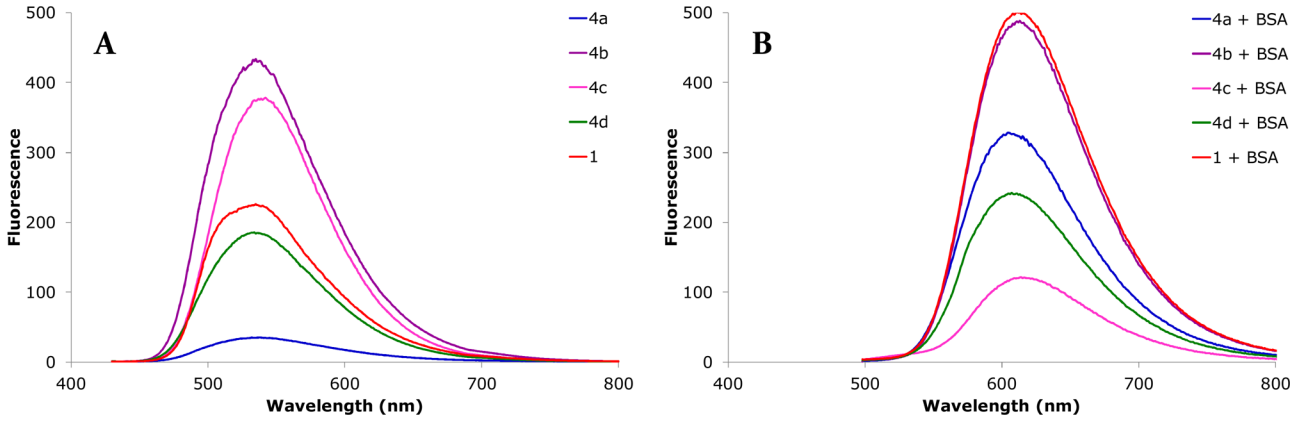

Figure 1. Emission spectra of epicocconone (**1**) and analogues **4a−d** in water at pH 2.5 with 0.1% SDS in the (A) absence or (B) presence of excess protein (BSA). All spectra are normalized on identical concentrations of fluorophores (10 μM) and for excitation at the longest λ_{ex} (Table 2).

dx.doi.org/10.1021/ja506914p | J. Am. Chem. Soc. 2014, 136, 15248−15256

Table 2. Relative Quantum Yields, Molar Extinction Coefficients, and Brightnesses of Epicocconone (1) and Analogues 4a–d, 12a–d, and 17a–d in H_2O (pH 2.5) with 0.1% SDS in the Absence or Presence of Excess Protein (BSA)

	without BSA					with BSA				
compd	λ_{ex}[a] (nm)	λ_{em} (nm)	ε (M^{-1} cm^{-1})	Φ_F[b] (%)	brightness[c] (M^{-1} cm^{-1})	λ_{ex}[d] (nm)	λ_{em} (nm)	ε (M^{-1} cm^{-1})	Φ_F[e] (%)	brightness[c] (M^{-1} cm^{-1})
1	258, 319, 444	535	68600	7.4 ± 0.2	5.08	256, 370, 518	611	26400	17.1 ± 0.2	4.51
4a	253, 303, 420	538	17600	4.8 ± 0.2	0.85	258, 369, 509	605	11600	21.7 ± 0.5	2.52
4b	252, 308, 435	538	39200	19.8 ± 0.4	7.76	255, 372, 518	613	18400	21.2 ± 0.7	3.90
4c	252, 312, 425	542	11300	40.3 ± 0.2	4.55	254, 370, 527	614	5500	16.7 ± 0.5	0.91
4d	254, 303, 417	534	14500	27.0 ± 0.4	3.92	257, 370, 518	607	10800	18.8 ± 0.5	2.03
12a	260, 320, 383	519	4000	2.8 ± 0.2	0.11	257, 345, 480	589	700	4.5 ± 0.1	0.03
12b	262, 317, 381	520	2200	3.0 ± 0.1	0.07	247, 347, 477	587	300	5.8 ± 0.2	0.02
12d	308, 383	526	2000	13.4 ± 0.2	0.27	260, 352, 477	589	300	2.8 ± 0.1	0.01
17a	279, 391	517	8800	34.6 ± 0.7	3.05	271, 350, 485	586	5100	3.5 ± 0.1	0.18
17d	248, 322, 392	518	13200	40.1 ± 1.0	5.29	250, 353, 492	587	2600	3.0 ± 0.1	0.08

[a]Excitation spectrum recorded with emission at 520 nm. [b]Quantum yield relative to Lucifer Yellow CH (Φ_F = 0.21) ± standard deviation of three readings. [c]Brightness is defined as $\Phi_F \times \varepsilon/1000$. [d]Excitation spectrum recorded with emission at 620 nm. [e]Relative to rhodamine 6G (Φ_F = 0.76); see Figure S4 in the Supporting Information.

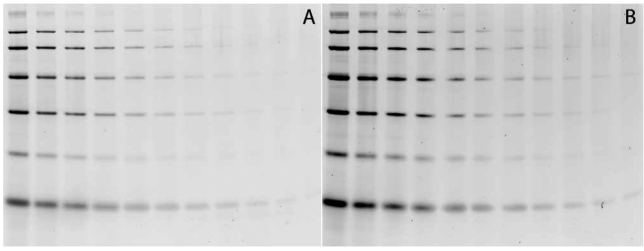

Figure 2. 1D gels stained with (A) Deep Purple and (B) compound **4b** run and scanned under identical conditions with similar concentrations of dye (~1 μg/mL in each case).

Table 3. Limits of Detection (pg) for Analogues 4a–d and Deep Purple (Epicocconone 1) in 1D Gel Electrophoresis

	1	4a	4b	4c	4d
phosphorylase B	1838	2562	799	1534	1393
albumin	917	1301	560	1005	1123
ovalbumin	1766	668	763	1210	866
carbonic anhydrase	877	838	593	864	655
soybean trypsin inhibitor	1338	1763	786	401	893

more spots than Deep Purple (Table S3 in the Supporting Information) under the same illumination conditions, allowing a much deeper analysis of the proteome. In 2D gels, Deep Purple performs well on low-molecular-weight and basic proteins. Analogue **4b** had similar characteristics but resulted in better staining of acidic proteins (left-hand side of the gel). However, in general the staining characteristics of **4b** and **1** were very similar, as expected.

In comparison to Sypro Ruby, **4b** had substantially lower levels of noise, better peak shapes, and less speckling (Figure 4). The staining profiles were quite similar for the two dyes, in accordance with the fixation targets of the fluorescent probes (lysines for epicocconone and its analogues and basic residues

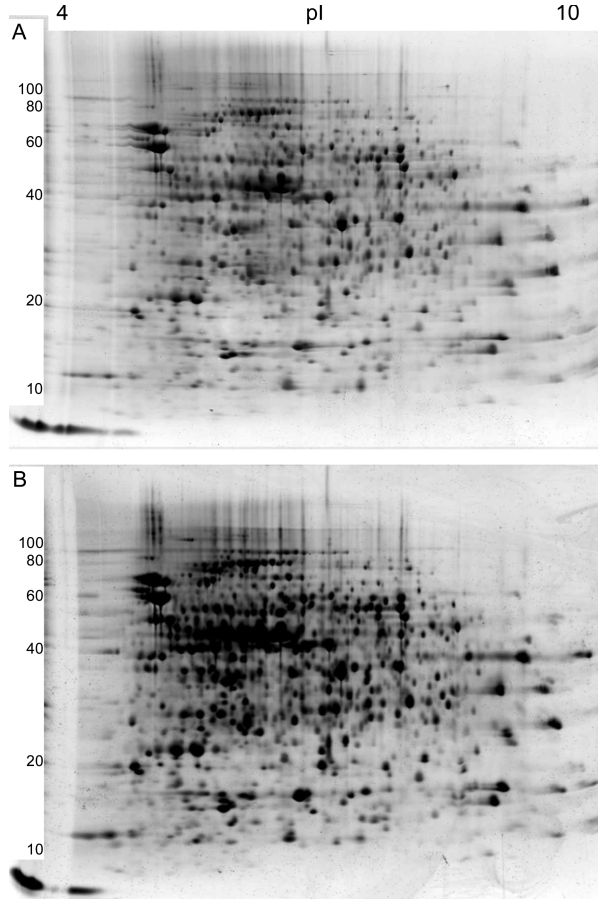

Figure 3. 2D gel electrophoresis (pH 3–10) of the *E. coli* proteome stained with (A) Deep Purple Total Protein Stain and (B) compound **4b**. Identical concentrations of dye were used in the two gels (1 μg/mL).

dx.doi.org/10.1021/ja506914p | J. Am. Chem. Soc. 2014, 136, 15248–15256

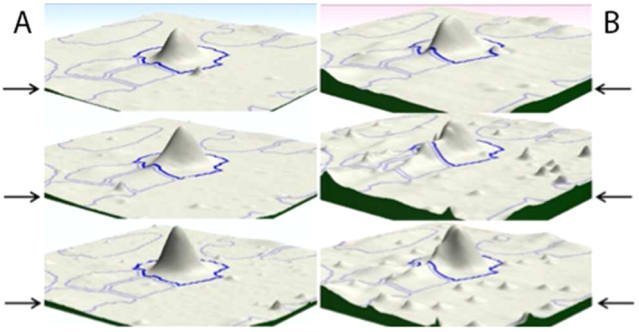

Figure 4. Details of the 2D gels (triplicates) comparing the background peak intensities (arrows), slopes, and surface textures for (A) **4b** and (B) Sypro Ruby.

for Sypro Ruby). However, there were some noteworthy differences in staining that were further investigated by mass spectrometry. We found that 10 spots (eight proteins) were stained more intensely with Sypro Ruby but 21 spots (16 proteins) were stained more intensely with **4b** (Figure S12 in the Supporting Information). Identification of these differentially stained proteins showed that neither the aliphatic index nor the hydropathy value explained the differential labeling (Table 4). The contents of amino acids were then compared.

Table 4. Statistical Analysis of Differential Staining Between 4b and Sypro Ruby (SR)

	mean ± SE		
	4b	SR	*p* value
aliphatic index	92.6 ± 1.7	90.2 ± 1.8	0.393
hydropathy	−0.226 ± 0.061	−0.143 ± 0.056	0.384
percentage Lys	0.077 ± 0.005	0.047 ± 0.007	0.001
percentage Arg	0.047 ± 0.006	0.063 ± 0.010	0.145
percentage His	0.012 ± 0.002	0.030 ± 0.005	0.0006

As might be expected, the percentage of lysine was higher for protein spots specifically stained with **4b** (p = 0.001). In contrast, Sypro Ruby was more sensitive to histidine content (p = 0.0006), a feature that has not been reported previously. This underlines the fact that epicocconone analogues more heavily label proteins that are rich in lysines and that Sypro Ruby (a ruthenium complex)[4] could be expected to complex histidine-rich proteins.

As Deep Purple has been noted to suffer from photobleaching when used to manually pick protein spots from gels using a transilluminator, we were keen to assess the performance of the analogues to see whether replacement of the triene improved their photostability. Repeating the work of Smejkal,[11] we found Deep Purple, which contains epicocconone (**1**), to have a half-life of 11 min over 60 W UV irradiation as previously reported. The influence of substitution on the photostability is clearly shown by the observations that compound **4a** (with an electron-rich *p*-anisyl substituent) was photobleached faster than **1** whereas electron-poor **4b** (naphthyl group, $t_{1/2}$ = 33 min) and **4c** (2-chloropyridyl group, $t_{1/2}$ = 45 min) were substantially more stable than **1** (Figure 5). These results clearly show the influence of the side chain on the photostability even though the side chain is not directly part of the emissive S_1 state (Figure 1). An interesting observation was that for **4b** the signal-to-noise ratio (S/N) actually increased with time (Figure S9 in the Supporting Information), indicating that the underivatized dye in the background of the gel is bleached faster by UV light than the stain colocated with protein. This may be due to the fact that **4b** has significant fluorescence even in the absence of protein (Figure 1A), leading initially to a high background (where there is no protein) in gels stained with this analogue. Meanwhile, the enamine of **4b** formed in the presence of protein is more stable toward photobleaching than free **4b**, leading to an increase in S/N over time.

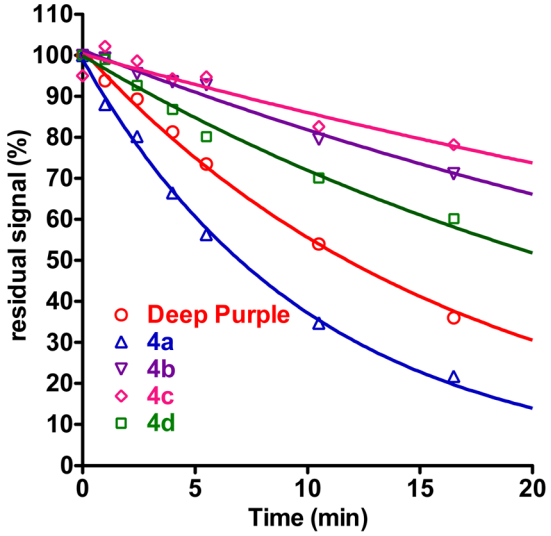

Figure 5. Photobleaching studies of Deep Purple (containing **1**) and epicocconone analogues **4a–d**.

CONCLUSIONS

In conclusion, we have taken the first approaches to the total synthesis of the natural product epicocconone (**1**) by preparing, in five steps, several analogues that possess distinct advantages over the natural product in terms of quantum yield and stability. The synthesis design is general and straightforward, providing facile access to libraries of polyfunctional fluorophores with large Stokes shifts based on a lead from nature. The resulting epicocconone analogues, especially **4b**, were found to be excellent latent fluorophores that are useful in protein detection in 1D and 2D gel electrophoresis with superior sensitivity and stability compared with the leading commercial products Sypro Ruby and Deep Purple, respectively. These enhanced detection properties are expected to enable new protein discovery opportunities. For example, a gel stain better than Deep Purple with a biotin tag will open a new dimension of practical applications to visualize proteins in gels and on membranes, beads, or protein arrays. Such biotin affinity tags will also enable the isolatation, purification, manipulation, processing, and analysis of captured proteins that otherwise would escape detection.

EXPERIMENTAL SECTION

Synthesis. See the Supporting Information

DFT Calculations. DFT calculations were run using Turbomole 6.6 (Cosmologic GmbH & Co). Theoretical ground-state geometries for all conformations were calculated at the DFT-D3//BP86/TZVPP level[19c,d,25] using a continuum solvent model (COSMO)[20] for toluene. Frequency analysis confirmed that all structures were stationary points.

1D Gel Electrophoresis. The 12% Bis-Tris Novex NuPage (Invitrogen, NP0342BOX) 1 mm thick gels were loaded with the dilution series (5 μL) of GE low-molecular-weight markers (GE

dx.doi.org/10.1021/ja506914p | J. Am. Chem. Soc. 2014, 136, 15248−15256

Healthcare, 17-0446-01) to obtain the concentrations indicated in Table S1 in the Supporting Information. The gels were run in Xcell SureLock minigel systems (Invitrogen, EI0001) at 150 V for approximately 65 min (buffer front just off gel) using MES buffer (50 mM MES, 50 mM Tris, 1 mM EDTA, 0.1% SDS, pH 7.3). The gels were then removed and fixed in 15% (v/v) ethanol with 1% (w/v) citric acid (100 mL) on a rocker for 1 h and then overnight with fresh fixative. The next day, gels were placed into fresh fixative (100 mL) for 1 h, drained, and then stained in 100 mM sodium borate buffer (50 mL; pH 10.9) containing either Deep Purple Total Protein Stain (GE Healthcare, RPN6306; 250 μL) or one of the analogues (50 μL of a 1 mg/mL solution in DMSO). These concentrations resulted in approximately 1 μg/mL active fluorophore in each case. After 1 h of staining, the gels were destained in 15% ethanol (100 mL) for 30 min and transferred back into fresh fixative [100 mL; 15% (v/v) ethanol, 1% (w/v) citric acid] for 30 min. All of the gels were imaged using a Typhoon Trio imager (GE, 63-0055-87) with a 532 nm Nd:YAG laser, 540 PMT, 610BP30 filter, 100 μm resolution, and normal sensitivity. The Typhoon scans (.gel files) were analyzed using IMageQuantTL (v7, GE Healthcare), and band volumes and background were calculated using the 1D gel band analysis package (Figures S5 and S6 in the Supporting Information).

Photobleaching. 1D gels (as above) were subjected to UV light by placing them onto a standard transilluminator (4 × 15 W; 312 nm tubes). The gels were imaged after each interval and then placed back into cold fixative (100 mL) for 3 min to allow them to cool. Each gel was exposed to UV light for 60, 146, 240, 330, 630, and 990 s (cumulative exposure). The Typhoon scans (.gel files; Figures S7 and S8 in the Supporting Information) were analyzed using IMageQuantTL (v7, GE healthcare), and band volumes and background (between bands) were calculated using IMageQuantTL. The average volume of each protein band over background was fitted to a one-phase exponential decay (Graphpad Prism v5.0), and the pseudo-first-order decays rate was calculated.

2D Gel Electrophoresis. Four 24 cm pI 3−10 Immobiline dry strips (GE Healthcare, 17-1234-01) were rehydrated into IEF buffer (40 mM Tris-HCl, 2 M thiourea, 5 M urea, 2% CHAPS, 2% sulfobetaine 3−10, 0.002% bromophenol blue; 180 μL per IPG strip) containing whole-cell lysate from *Escherichia coli* (100 μg per IPG strip) for 6 h by laying the strips gel down in a rehydration tray. The strips were then focused for 48 000 V h using an IPGphor 3 power pack (GE Healthcare, 11-0033-64) before being stored at −80 °C. The strips were equilibrated using equilibration buffer (GelCompany, 1019-20; 2 × 10 mL) for 2 × 15 min; the first equilibration also contained 1% (w/v) DTT, while the second contained 5% (w/v) iodoacetamide. Separation in the second dimension was performed with a flatbed Tower electrophoresis unit (Serva, HPE-TS1.01) using the standard manufacturer's protocol. 2DGel flatbed 12.5% acrylamide gels (250 mm × 200 mm × 0.65 mm) from GelCompany (1019-02) were used following the standard protocol. Briefly, focused IPG strips were removed from the IAA solution and placed gel side down onto the stacking gel portion of the 2D gels. Proteins were transferred to the 2D gel (100 V/28 mA/30 min, 200 V/52 mA/30 min, 300 V/80 mA/10 min), and then the IPG strip was removed. The 2D gel was run at 15 °C (1500 V/160 mA) for 3.5 h. The gels were then removed, fixed in 15% (v/v) ethanol, 1% (w/v) citric acid (500 mL) on a rocker for 90 min, and then stained in 100 mM sodium borate buffer (350 mL; pH 10.9) with either Deep Purple Total Protein Stain (GE Healthcare, RPN6306; gel A 1.00 mL, gel B 1.75 mL) or analogue **4b** (gel C 350 μL; gel D 100 μL of a 1 mg/mL solution in DMSO). Gels B and C (Figure S10 in the Supporting Information) both had a final dye concentration of ∼1 μg/mL in the staining solution. After 1 h of staining, the gels were destained in 15% (v/v) ethanol (500 mL) for 45 min and transferred to fixative [500 mL; 15% (v/v) ethanol, 1% (w/v) citric acid] for 45 min. All of the gels were imaged using a Typhoon Trio imager (GE, 63-0055-87) with a 532 nm Nd:YAG laser, 540 PMT, 610BP30 filter, 100 μm resolution, and normal sensitivity.

Sypro Ruby 2D gels were run on a Protean II xi cell (Bio-Rad) using a 12.5% (w/v) polyacrylamide resolving gel (width, 16 cm; length, 20 cm; thickness, 0.75 mm). Triplicate gels were fixed overnight, and proteins were stained using Sypro Ruby according to the manufacturer's protocol or as above for compound **4b** (Figure S12 in the Supporting Information). Gels were scanned using a ProXpress fluorimager (PerkinElmer) and analyzed using SameSpots 4.0 software (Nonlinear Dynamics), and all triplicate images were aligned before analysis. Gels were stored in water at 4 °C before spot excision.

Protein Identification. After excision of protein spots from 2D gels, the fragments were washed with water and dried in a SpeedVac centrifuge for a few minutes. Trypsin digestion (with 10 μL of a 10 ng/μL trypsin solution, Promega) was performed overnight (PerkinElmer, MultiPROBE II). The peptides were extracted with H_2O/CH_3CN (1:1) for 2 × 15 min, dried, and solubilized in 3% CH_3CN/0.1% HCOOH/water. The peptides were concentrated and separated by reversed-phase HPLC with a precolumn/analytical column nanoflow setup (Agilent, HPLC-Chip cube). The peptides were analyzed by LC−MS and further fragmented after a full survey scan (m/z 300−2000) using an online QTOF mass spectrometer (Agilent, 6520). MS/MS experiments on the five most abundant precursor ions were performed, and the fragmentation data were exported using the MassHunter qualitative analysis module (Agilent, version B.02.00).

For protein identification, extracted MS/MS peak lists were compared to the MSDB database restricted to the *E. coli* ORF protein database (31797) using the MASCOT Daemon (version 2.1.3) search engine. All searches were performed with no fixed modification and with variable modifications for carbamidomethylation of cysteines and for oxidation of methionines, with a maximum of one missed cleavage. MS2 spectra were searched with a mass tolerance of 5 ppm for precursor ions and 0.02 Da for fragment ions, respectively. The protein identification was validated if two peptides exhibited fragmentation profile scores higher than the average default value for significance using MASCOT. For sequence analysis, ProtParam (http://web.expasy.org/protparam/) was used to calculate the amino acid composition, aliphatic index, and grand average of hydropathicity (GRAVY). The aliphatic index of a protein is defined as the relative volume occupied by aliphatic side chains (alanine, valine, isoleucine, and leucine). The GRAVY value for a protein was calculated as the sum of the hydropathy values of all the amino acids divided by the number of residues in the sequence.

■ ASSOCIATED CONTENT

Supporting Information

Synthetic procedures, NMR spectra, fluorescence data, gel images, and analyses of gel images. This material is available free of charge via the Internet at http://pubs.acs.org.

■ AUTHOR INFORMATION

Corresponding Authors

peter.karuso@mq.edu.au
xavier.franck@insa-rouen.fr

Notes

The authors declare no competing financial interest.

■ ACKNOWLEDGMENTS

We gratefully acknowledge the Région Haute Normandie for financial support to P.A.P. and A.B and the ANR-BLAN-732-01 grant for financial support and the Australian Research Council for support of P.K. We thank the Ministère des Affaires Etrangères (France) and the Department of Innovation, Industry, Science and Research (Australia) for FAST Grants. This research was facilitated by access to the Australian Proteome Analysis Facility established under the Australian Government's Major National Research Facilities Program. The authors thank Kent Taylor (Gratuk Technologies) for running the 2D gels. Dr. Fei Liu (Macquarie University) is acknowledged for helpful discussions.

REFERENCES

(1) Udenfriend, S.; Stein, S.; Böhlen, P.; Dairman, W.; Leimgruber, W.; Weigele, M. *Science* **1972**, *178*, 871−872.
(2) Chandran, S. S.; Dickson, K. A.; Raines, R. T. *J. Am. Chem. Soc.* **2005**, *127*, 1652−1653.
(3) Girouard, S.; Houle, M. H.; Grandbois, A.; Keillor, J. W.; Michnick, S. W. *J. Am. Chem. Soc.* **2005**, *127*, 559−566.
(4) Ball, M. S.; Karuso, P. *J. Proteome Res.* **2007**, *6*, 4313−4320.
(5) Bell, P. J. L.; Karuso, P. *J. Am. Chem. Soc.* **2003**, *125*, 9304−9305.
(6) (a) Moritz, C. P.; Marz, S. X.; Reiss, R.; Schulenborg, T.; Friauf, E. *Proteomics* **2014**, *14*, 162−168. (b) Tang, W. *Methods Mol. Biol.* **2012**, *876*, 67−82. (c) Liu, H.; Crooks, R. M. *J. Am. Chem. Soc.* **2011**, *133*, 17564−17566. (d) Steinberg, T. H. *Methods Enzymol.* **2009**, *463*, 541−563. (e) Karp, N. A.; Feret, R.; Rubtsov, D. V.; Lilley, K. S. *Proteomics* **2008**, *8*, 948−960. (f) Karuso, P.; Crawford, A. S.; Veal, D. A.; Scott, G. B. I.; Choi, H.-Y. *J. Proteome Res.* **2008**, *7*, 361−366. (g) Choi, H. Y.; Veal, D. A.; Karuso, P. *J. Fluoresc.* **2006**, *16*, 475−482. (h) Mackintosh, J. A.; Veal, D. A.; Karuso, P. *Proteomics* **2005**, *5*, 4673−4677. (i) Mackintosh, J. A.; Choi, H.-Y.; Bae, S.-H.; Veal, D. A.; Bell, P. J.; Ferrari, B. C.; Van Dyk, D. D.; Verrills, N. M.; Paik, Y.-K.; Karuso, P. *Proteomics* **2003**, *3*, 2273−2288.
(7) Coghlan, D. R.; Mackintosh, J. A.; Karuso, P. *Org. Lett.* **2005**, *7*, 2401−2404.
(8) (a) Chatterjee, S.; Burai, T. N.; Karuso, P.; Datta, A. *J. Phys. Chem. A* **2011**, *115*, 10154−10158. (b) Panda, D.; Datta, A. *J. Chem. Sci.* **2007**, *119*, 99−104.
(9) Haugland, R. P. *Handbook of Fluorescent Probes and Research Products*, 9th ed.; Molecular Probes: Eugene, OR, 2002.
(10) *Molecular Probes Handbook—A Guide to Fluorescent Probes and Labeling Technologies*, 11th ed.; Life Technologies: Eugene, OR, 2010.
(11) Smejkal, G. B.; Robinson, M. H.; Lazarev, A. *Electrophoresis* **2004**, *25*, 2511−2519.
(12) Garavelli, M.; Celani, P.; Yamamoto, N.; Bernardi, F.; Robb, M. A.; Olivucci, M. *J. Am. Chem. Soc.* **1996**, *118*, 11656−11657.
(13) Hirashima, S.-i.; Itoh, A. *Green Chem.* **2007**, *9*, 318−320.
(14) (a) Millioni, R.; Tolin, S.; Sbrignadello, S.; Fadini, G.; Puricelli, L.; Tessari, P.; Arrigoni, G. *Nutr., Metab. Cardiovasc. Dis.* **2013**, *23*, S54−S55. (b) Fey, S. J.; Larsen, P. M. *Curr. Opin. Chem. Biol.* **2001**, *5*, 26−33. (c) Wang, H.; Chang-Wong, T.; Tang, H.-Y.; Speicher, D. W. *J. Proteome Res.* **2010**, *9*, 1032−1040. (d) Beseme, O.; Fertin, M.; Drobecq, H.; Amouyel, P.; Pinet, F. *Electrophoresis* **2010**, *31*, 2697−2704.
(15) (a) Roche, S. P.; Porco, J. A., Jr. *Angew. Chem., Int. Ed.* **2011**, *50*, 4068−4093. (b) Van De Water, R. W.; Hoarau, C.; Pettus, T. R. *Tetrahedron Lett.* **2003**, *44*, 5109−5113.
(16) (a) Boulangé, A.; Peixoto, P. A.; Franck, X. *Chem.—Eur. J.* **2011**, *17*, 10241−10245. (b) Franck, X.; Peixoto, P.; Karuso, P. H. (Universite de Rouen, France; Macquarie University, Australia). Process for Synthesizing Epicocconone Analogues as Fluorescent Dyes. WO2011051225A1, 2011. (c) Lebrasseur, N.; Gagnepain, J.; Ozanne-Beaudenon, A.; Leger, J. M.; Quideau, S. *J. Org. Chem.* **2007**, *72*, 6280−6283.
(17) Reber, K. P.; Tilley, S. D.; Sorensen, E. J. *Chem. Soc. Rev.* **2009**, *38*, 3022−3034.
(18) (a) Carroll, M. F.; Bader, A. R. *J. Am. Chem. Soc.* **1953**, *75*, 5400−5402. (b) Peixoto, P. A.; Boulangé, A.; Leleu, S.; Franck, X. *Eur. J. Org. Chem.* **2013**, 3316−3327.
(19) (a) Treutler, O.; Ahlrichs, R. *J. Chem. Phys.* **1995**, *102*, 346−354. (b) Eichkorn, K.; Weigend, F.; Treutler, O.; Ahlrichs, R. *Theor. Chem. Acc.* **1997**, *97*, 119−124. (c) Weigend, F.; Ahlrichs, R. *Phys. Chem. Chem. Phys.* **2005**, *7*, 3297−3305. (d) Grimme, S.; Antony, J.; Ehrlich, S.; Krieg, H. *J. Chem. Phys.* **2010**, *132*, No. 154104.
(20) Klamt, A.; Schüürmann, G. *J. Chem. Soc., Perkin Trans. 2* **1993**, 799−805.
(21) (a) Syzgantseva, O. A.; Tognetti, V.; Boulangé, A.; Peixoto, P. A.; Leleu, S.; Franck, X.; Joubert, L. *J. Phys. Chem. A* **2014**, *118*, 757−764. (b) Syzgantseva, O. A.; Tognetti, V.; Joubert, L.; Boulangé, A.; Peixoto, P. A.; Leleu, S.; Franck, X. *J. Phys. Chem. A* **2012**, *116*, 8634−8643.
(22) Chatterjee, S.; Karuso, P.; Boulangé, A.; Peixoto, P. A.; Franck, X.; Datta, A. *J. Phys. Chem. B* **2013**, *117*, 14951−14959.
(23) Deep Purple is a commercial product from GE Healthcare consisting of ∼1.8% epicocconone specially formulated for 1D and 2D protein gel staining. The stain has high sensitivity when scanned with either a 488 or 532 nm laser scanner. See: http://www.fluorotechnics.com.au/pdf/dige_compat.pdf (accessed July 11, 2014).
(24) Berggren, K.; Chernokalskaya, E.; Steinberg, T. H.; Kemper, C.; Lopez, M. F.; Diwu, Z.; Haugland, R. P.; Patton, W. F. *Electrophoresis* **2000**, *21*, 2509−2521.
(25) Bauernschmitt, R.; Haser, M.; Treutler, O.; Ahlrichs, R. *Chem. Phys. Lett.* **1997**, *264*, 573−578.